Precision Measurement of the $e^+e^- \to \Lambda_c^+ \bar{\Lambda}_c^-$ Cross Section Near Threshold

M. Ablikim,[1] M. N. Achasov,[9,d] S. Ahmed,[14] M. Albrecht,[4] M. Alekseev,[55a,55c] A. Amoroso,[55a,55c] F. F. An,[1] Q. An,[52,42] J. Z. Bai,[1] Y. Bai,[41] O. Bakina,[26] R. Baldini Ferroli,[22a] Y. Ban,[34] K. Begzsuren,[24] D. W. Bennett,[21] J. V. Bennett,[5] N. Berger,[25] M. Bertani,[22a] D. Bettoni,[23a] F. Bianchi,[55a,55c] E. Boger,[26,b] I. Boyko,[26] R. A. Briere,[5] H. Cai,[57] X. Cai,[1,42] O. Cakir,[45a] A. Calcaterra,[22a] G. F. Cao,[1,46] S. A. Cetin,[45b] J. Chai,[55c] J. F. Chang,[1,42] G. Chelkov,[26,b,c] G. Chen,[1] H. S. Chen,[1,46] J. C. Chen,[1] M. L. Chen,[1,42] P. L. Chen,[53] S. J. Chen,[32] X. R. Chen,[29] Y. B. Chen,[1,42] X. K. Chu,[34] G. Cibinetto,[23a] F. Cossio,[55c] H. L. Dai,[1,42] J. P. Dai,[37,h] A. Dbeyssi,[14] D. Dedovich,[26] Z. Y. Deng,[1] A. Denig,[25] I. Denysenko,[26] M. Destefanis,[55a,55c] F. De Mori,[55a,55c] Y. Ding,[30] C. Dong,[33] J. Dong,[1,42] L. Y. Dong,[1,46] M. Y. Dong,[1,42,46] Z. L. Dou,[32] S. X. Du,[60] P. F. Duan,[1] J. Fang,[1,42] S. S. Fang,[1,46] Y. Fang,[1] R. Farinelli,[23a,23b] L. Fava,[55b,55c] S. Fegan,[25] F. Feldbauer,[4] G. Felici,[22a] C. Q. Feng,[52,42] E. Fioravanti,[23a] M. Fritsch,[4] C. D. Fu,[1] Q. Gao,[1] X. L. Gao,[52,42] Y. Gao,[44] Y. G. Gao,[6] Z. Gao,[52,42] B. Garillon,[25] I. Garzia,[23a] A. Gilman,[49] K. Goetzen,[10] L. Gong,[33] W. X. Gong,[1,42] W. Gradl,[25] M. Greco,[55a,55c] M. H. Gu,[1,42] Y. T. Gu,[12] A. Q. Guo,[1] R. P. Guo,[1,46] Y. P. Guo,[25] A. Guskov,[26] Z. Haddadi,[28] S. Han,[57] X. Q. Hao,[15] F. A. Harris,[47] K. L. He,[1,46] X. Q. He,[51] F. H. Heinsius,[4] T. Held,[4] Y. K. Heng,[1,42,46] T. Holtmann,[4] Z. L. Hou,[1] H. M. Hu,[1,46] J. F. Hu,[37,h] T. Hu,[1,42,46] Y. Hu,[1] G. S. Huang,[52,42] J. S. Huang,[15] X. T. Huang,[36] X. Z. Huang,[32] Z. L. Huang,[30] T. Hussain,[54] W. Ikegami Andersson,[56] Q. Ji,[1] Q. P. Ji,[15] X. B. Ji,[1,46] X. L. Ji,[1,42] X. S. Jiang,[1,42,46] X. Y. Jiang,[33] J. B. Jiao,[36] Z. Jiao,[17] D. P. Jin,[1,42,46] S. Jin,[1,46] Y. Jin,[48] T. Johansson,[56] A. Julin,[49] N. Kalantar-Nayestanaki,[28] X. S. Kang,[33] M. Kavatsyuk,[28] B. C. Ke,[1] T. Khan,[52,42] A. Khoukaz,[50] P. Kiese,[25] R. Kliemt,[10] L. Koch,[27] O. B. Kolcu,[45b,f] B. Kopf,[4] M. Kornicer,[47] M. Kuemmel,[4] M. Kuhlmann,[4] A. Kupsc,[56] W. Kühn,[27] J. S. Lange,[27] M. Lara,[21] P. Larin,[14] L. Lavezzi,[55c] H. Leithoff,[25] C. Li,[56] Cheng Li,[52,42] D. M. Li,[60] F. Li,[1,42] F. Y. Li,[34] G. Li,[1] H. B. Li,[1,46] H. J. Li,[1,46] J. C. Li,[1] J. W. Li,[40] Jin Li,[35] K. J. Li,[43] Kang Li,[13] Ke Li,[1] Lei Li,[3] P. L. Li,[52,42] P. R. Li,[46,7] Q. Y. Li,[36] W. D. Li,[1,46] W. G. Li,[1] X. L. Li,[36] X. N. Li,[1,42] X. Q. Li,[33] Z. B. Li,[43] H. Liang,[52,42] Y. F. Liang,[39] Y. T. Liang,[27] G. R. Liao,[11] J. Libby,[20] C. X. Lin,[43] D. X. Lin,[14] B. Liu,[37,h] B. J. Liu,[1] C. X. Liu,[1] D. Liu,[52,42] F. H. Liu,[38] Fang Liu,[1] Feng Liu,[6] H. B. Liu,[12] H. L. Liu,[41] H. M. Liu,[1,46] Huanhuan Liu,[1] Huihui Liu,[16] J. B. Liu,[52,42] J. Y. Liu,[1,46] K. Liu,[44] K. Y. Liu,[30] Ke Liu,[6] L. D. Liu,[34] Q. Liu,[46] S. B. Liu,[52,42] X. Liu,[29] Y. B. Liu,[33] Z. A. Liu,[1,42,46] Zhiqing Liu,[25] Y. F. Long,[34] X. C. Lou,[1,42,46] H. J. Lu,[17] J. G. Lu,[1,42] Y. Lu,[1] Y. P. Lu,[1,42] C. L. Luo,[31] M. X. Luo,[59] X. L. Luo,[1,42] S. Lusso,[55c] X. R. Lyu,[46] F. C. Ma,[30] H. L. Ma,[1] L. L. Ma,[36] M. M. Ma,[1,46] Q. M. Ma,[1] T. Ma,[1] X. N. Ma,[33] X. Y. Ma,[1,42] Y. M. Ma,[36] F. E. Maas,[14] M. Maggiora,[55a,55c] Q. A. Malik,[54] Y. J. Mao,[34] Z. P. Mao,[1] S. Marcello,[55a,55c] Z. X. Meng,[48] J. G. Messchendorp,[28] G. Mezzadri,[23b] J. Min,[1,42] R. E. Mitchell,[21] X. H. Mo,[1,42,46] Y. J. Mo,[6] C. Morales Morales,[14] N. Yu. Muchnoi,[9,d] H. Muramatsu,[49] A. Mustafa,[4] Y. Nefedov,[26] F. Nerling,[10] I. B. Nikolaev,[9,d] Z. Ning,[1,42] S. Nisar,[8] S. L. Niu,[1,42] X. Y. Niu,[1,46] S. L. Olsen,[35] Q. Ouyang,[1,42,46] S. Pacetti,[22b] Y. Pan,[52,42] M. Papenbrock,[56] P. Patteri,[22a] M. Pelizaeus,[4] J. Pellegrino,[55a,55c] H. P. Peng,[52,42] Z. Y. Peng,[12] K. Peters,[10,g] J. Pettersson,[56] J. L. Ping,[31] R. G. Ping,[1,46] A. Pitka,[4] R. Poling,[49] V. Prasad,[52,42] H. R. Qi,[2] M. Qi,[32] T. Y. Qi,[2] S. Qian,[1,42] C. F. Qiao,[46] N. Qin,[57] X. S. Qin,[4] Z. H. Qin,[1,42] J. F. Qiu,[1] K. H. Rashid,[54,i] C. F. Redmer,[25] M. Richter,[4] M. Ripka,[25] M. Rolo,[55c] G. Rong,[1,46] Ch. Rosner,[14] A. Sarantsev,[26,e] M. Savrié,[23b] C. Schnier,[4] K. Schoenning,[56] W. Shan,[18] X. Y. Shan,[52,42] M. Shao,[52,42] C. P. Shen,[2] P. X. Shen,[33] X. Y. Shen,[1,46] H. Y. Sheng,[1] X. Shi,[1,42] J. J. Song,[36] W. M. Song,[36] X. Y. Song,[1] S. Sosio,[55a,55c] C. Sowa,[4] S. Spataro,[55a,55c] G. X. Sun,[1] J. F. Sun,[15] L. Sun,[57] S. S. Sun,[1,46] X. H. Sun,[1] Y. J. Sun,[52,42] Y. K. Sun,[52,42] Y. Z. Sun,[1] Z. J. Sun,[1,42] Z. T. Sun,[21] Y. T. Tan,[52,42] C. J. Tang,[39] G. Y. Tang,[1] X. Tang,[1] I. Tapan,[45c] M. Tiemens,[28] B. Tsednee,[24] I. Uman,[45d] G. S. Varner,[47] B. Wang,[1] B. L. Wang,[46] D. Wang,[34] D. Y. Wang,[34] Dan Wang,[46] K. Wang,[1,42] L. L. Wang,[1] L. S. Wang,[1] M. Wang,[36] Meng Wang,[1,46] P. Wang,[1] P. L. Wang,[1] W. P. Wang,[52,42] X. F. Wang,[44] Y. Wang,[52,42] Y. D. Wang,[14] Y. F. Wang,[1,42,46] Y. Q. Wang,[25] Z. Wang,[1,42] Z. G. Wang,[1,42] Z. Y. Wang,[1] Zongyuan Wang,[1,46] T. Weber,[4] D. H. Wei,[11] J. H. Wei,[33] P. Weidenkaff,[25] S. P. Wen,[1] U. Wiedner,[4] M. Wolke,[56] L. H. Wu,[1] L. J. Wu,[1,46] Z. Wu,[1,42] L. Xia,[52,42] Y. Xia,[19] D. Xiao,[1] Y. J. Xiao,[1,46] Z. J. Xiao,[31] Y. G. Xie,[1,42] Y. H. Xie,[6] X. A. Xiong,[1,46] Q. L. Xiu,[1,42] G. F. Xu,[1] J. J. Xu,[1,46] L. Xu,[1] Q. J. Xu,[13] Q. N. Xu,[46] X. P. Xu,[40] F. Yan,[53] L. Yan,[55a,55c] W. B. Yan,[52,42] W. C. Yan,[2] Y. H. Yan,[19] H. J. Yang,[37,h] H. X. Yang,[1] L. Yang,[57] Y. H. Yang,[32] Y. X. Yang,[11] Yifan Yang,[1,46] M. Ye,[1,42] M. H. Ye,[7] J. H. Yin,[1] Z. Y. You,[43] B. X. Yu,[1,42,46] C. X. Yu,[33] J. S. Yu,[29] C. Z. Yuan,[1,46] Y. Yuan,[1] A. Yuncu,[45b,a] A. A. Zafar,[54] Y. Zeng,[19] Z. Zeng,[52,42] B. X. Zhang,[1] B. Y. Zhang,[1,42] C. C. Zhang,[1] D. H. Zhang,[1] H. H. Zhang,[43] H. Y. Zhang,[1,42] J. Zhang,[1,46] J. L. Zhang,[58] J. Q. Zhang,[4] J. W. Zhang,[1,42,46] J. Y. Zhang,[1] J. Z. Zhang,[1,46] K. Zhang,[1,46] L. Zhang,[44] S. Q. Zhang,[33] X. Y. Zhang,[36] Y. Zhang,[52,42] Y. H. Zhang,[1,42] Y. T. Zhang,[52,42] Yang Zhang,[1] Yao Zhang,[1] Yu Zhang,[46] Z. H. Zhang,[6] Z. P. Zhang,[52] Z. Y. Zhang,[57] G. Zhao,[1] J. W. Zhao,[1,42] J. Y. Zhao,[1,46] J. Z. Zhao,[1,42] Lei Zhao,[52,42] Ling Zhao,[1] M. G. Zhao,[33] Q. Zhao,[1] S. J. Zhao,[60] T. C. Zhao,[1] Y. B. Zhao,[1,42] Z. G. Zhao,[52,42] A. Zhemchugov,[26,b]

B. Zheng,[53,14] J. P. Zheng,[1,42] Y. H. Zheng,[46] B. Zhong,[31] L. Zhou,[1,42] Q. Zhou,[1,46] X. Zhou,[57] X. K. Zhou,[52,42] X. R. Zhou,[52,42] X. Y. Zhou,[1] A. N. Zhu,[1,46] J. Zhu,[43] K. Zhu,[1] K. J. Zhu,[1,42,46] S. Zhu,[1] S. H. Zhu,[51] X. L. Zhu,[44] Y. C. Zhu,[52,42] Y. S. Zhu,[1,46] Z. A. Zhu,[1,46] J. Zhuang,[1,42] B. S. Zou,[1] and J. H. Zou[1]

(BESIII Collaboration)

[1]*Institute of High Energy Physics, Beijing 100049, People's Republic of China*
[2]*Beihang University, Beijing 100191, People's Republic of China*
[3]*Beijing Institute of Petrochemical Technology, Beijing 102617, People's Republic of China*
[4]*Bochum Ruhr-University, D-44780 Bochum, Germany*
[5]*Carnegie Mellon University, Pittsburgh, Pennsylvania 15213, USA*
[6]*Central China Normal University, Wuhan 430079, People's Republic of China*
[7]*China Center of Advanced Science and Technology, Beijing 100190, People's Republic of China*
[8]*COMSATS Institute of Information Technology, Lahore, Defence Road, Off Raiwind Road, 54000 Lahore, Pakistan*
[9]*G. I. Budker Institute of Nuclear Physics SB RAS (BINP), Novosibirsk 630090, Russia*
[10]*GSI Helmholtzcentre for Heavy Ion Research GmbH, D-64291 Darmstadt, Germany*
[11]*Guangxi Normal University, Guilin 541004, People's Republic of China*
[12]*Guangxi University, Nanning 530004, People's Republic of China*
[13]*Hangzhou Normal University, Hangzhou 310036, People's Republic of China*
[14]*Helmholtz Institute Mainz, Johann-Joachim-Becher-Weg 45, D-55099 Mainz, Germany*
[15]*Henan Normal University, Xinxiang 453007, People's Republic of China*
[16]*Henan University of Science and Technology, Luoyang 471003, People's Republic of China*
[17]*Huangshan College, Huangshan 245000, People's Republic of China*
[18]*Hunan Normal University, Changsha 410081, People's Republic of China*
[19]*Hunan University, Changsha 410082, People's Republic of China*
[20]*Indian Institute of Technology Madras, Chennai 600036, India*
[21]*Indiana University, Bloomington, Indiana 47405, USA*
[22a]*INFN Laboratori Nazionali di Frascati, I-00044 Frascati, Italy*
[22b]*INFN and University of Perugia, I-06100 Perugia, Italy*
[23a]*INFN Sezione di Ferrara, I-44122 Ferrara, Italy*
[23b]*University of Ferrara, I-44122 Ferrara, Italy*
[24]*Institute of Physics and Technology, Peace Avenue 54B, Ulaanbaatar 13330, Mongolia*
[25]*Johannes Gutenberg University of Mainz, Johann-Joachim-Becher-Weg 45, D-55099 Mainz, Germany*
[26]*Joint Institute for Nuclear Research, 141980 Dubna, Moscow region, Russia*
[27]*Justus-Liebig-Universitaet Giessen, II. Physikalisches Institut, Heinrich-Buff-Ring 16, D-35392 Giessen, Germany*
[28]*KVI-CART, University of Groningen, NL-9747 AA Groningen, Netherlands*
[29]*Lanzhou University, Lanzhou 730000, People's Republic of China*
[30]*Liaoning University, Shenyang 110036, People's Republic of China*
[31]*Nanjing Normal University, Nanjing 210023, People's Republic of China*
[32]*Nanjing University, Nanjing 210093, People's Republic of China*
[33]*Nankai University, Tianjin 300071, People's Republic of China*
[34]*Peking University, Beijing 100871, People's Republic of China*
[35]*Seoul National University, Seoul 151-747, Korea*
[36]*Shandong University, Jinan 250100, People's Republic of China*
[37]*Shanghai Jiao Tong University, Shanghai 200240, People's Republic of China*
[38]*Shanxi University, Taiyuan 030006, People's Republic of China*
[39]*Sichuan University, Chengdu 610064, People's Republic of China*
[40]*Soochow University, Suzhou 215006, People's Republic of China*
[41]*Southeast University, Nanjing 211100, People's Republic of China*
[42]*State Key Laboratory of Particle Detection and Electronics, Beijing 100049, Hefei 230026, People's Republic of China*
[43]*Sun Yat-Sen University, Guangzhou 510275, People's Republic of China*
[44]*Tsinghua University, Beijing 100084, People's Republic of China*
[45a]*Ankara University, 06100 Tandogan, Ankara, Turkey*
[45b]*Istanbul Bilgi University, 34060 Eyup, Istanbul, Turkey*
[45c]*Uludag University, 16059 Bursa, Turkey*
[45d]*Near East University, Nicosia, North Cyprus, Mersin 10, Turkey*
[46]*University of Chinese Academy of Sciences, Beijing 100049, People's Republic of China*
[47]*University of Hawaii, Honolulu, Hawaii 96822, USA*
[48]*University of Jinan, Jinan 250022, People's Republic of China*

[49]University of Minnesota, Minneapolis, Minnesota 55455, USA
[50]University of Muenster, Wilhelm-Klemm-Straße 9, 48149 Muenster, Germany
[51]University of Science and Technology Liaoning, Anshan 114051, People's Republic of China
[52]University of Science and Technology of China, Hefei 230026, People's Republic of China
[53]University of South China, Hengyang 421001, People's Republic of China
[54]University of the Punjab, Lahore-54590, Pakistan
[55a]University of Turin, I-10125 Turin, Italy
[55b]University of Eastern Piedmont, I-15121 Alessandria, Italy
[55c]INFN, I-10125 Turin, Italy
[56]Uppsala University, Box 516, SE-75120 Uppsala, Sweden
[57]Wuhan University, Wuhan 430072, People's Republic of China
[58]Xinyang Normal University, Xinyang 464000, People's Republic of China
[59]Zhejiang University, Hangzhou 310027, People's Republic of China
[60]Zhengzhou University, Zhengzhou 450001, People's Republic of China

(Received 2 October 2017; revised manuscript received 18 December 2017; published 29 March 2018)

The cross section of the $e^+e^- \to \Lambda_c^+\bar{\Lambda}_c^-$ process is measured with unprecedented precision using data collected with the BESIII detector at $\sqrt{s} = 4574.5$, 4580.0, 4590.0 and 4599.5 MeV. The nonzero cross section near the $\Lambda_c^+\bar{\Lambda}_c^-$ production threshold is cleared. At center-of-mass energies $\sqrt{s} = 4574.5$ and 4599.5 MeV, the higher statistics data enable us to measure the Λ_c polar angle distributions. From these, the Λ_c electric over magnetic form-factor ratios ($|G_E/G_M|$) are measured for the first time. They are found to be $1.14 \pm 0.14 \pm 0.07$ and $1.23 \pm 0.05 \pm 0.03$, respectively, where the first uncertainties are statistical and the second are systematic.

DOI: 10.1103/PhysRevLett.120.132001

The electromagnetic structure of hadrons, parametrized in terms of electromagnetic form factors (EMFFs), provides a key to understanding quantum chromodynamics effects in bound states. The nucleon has been studied rigorously for more than sixty years, but new techniques and the availability of data with larger statistics from modern facilities have given rise to a renewed interest in the field, e.g., the proton radius puzzle [1]. Recently, the access to strange and charm hyperon structure by timelike EMFFs provides an additional dimension. Assuming that one-photon exchange dominates the production of spin-1/2 baryons B, the cross section of the process $e^+e^- \to B\bar{B}$ can be parametrized in terms of EMFFs, i.e., G_E and G_M, in the following way [2]:

$$\sigma_{B\bar{B}}(s) = \frac{4\pi\alpha^2 C\beta}{3s}|G_M(s)|^2\left(1 + \frac{2m_B^2c^4}{s}\left|\frac{G_E(s)}{G_M(s)}\right|^2\right). \quad (1)$$

Here, α is the fine-structure constant, $\beta = \sqrt{1 - 4m_B^2c^4/s}$ is the velocity of the baryon, s is the square of the center-of-mass (c.m.) energy, and m_B is the mass of the baryon. The Coulomb factor C parametrizes the electromagnetic interaction between the outgoing baryon and antibaryon. For neutral baryons, the Coulomb factor is unity, while for pointlike charged fermions it reads $C = \varepsilon R$ [3,4], where $\varepsilon = \pi\alpha/\beta$ is an enhancement factor resulting in a nonzero cross section at threshold, and $R = \sqrt{1-\beta^2}/(1 - e^{-\pi\alpha\sqrt{1-\beta^2}/\beta})$ is the Sommerfeld resummation factor [3]. The ratio of EMFFs associated with the polar angle distribution of the baryon can also parametrize the differential production cross section of the corresponding baryon [2].

In the $e^+e^- \to p\bar{p}$ process, the *BABAR* Collaboration observed a rapid rise of the cross section near threshold, followed by a plateau around 200 MeV above threshold [5]. The BESIII Collaboration also observed the cross-section enhancement [6]. The nonvanishing cross section near threshold as well as the wide-range plateau have led to various theoretical interpretations, including (i) final-state interactions [7], (ii) bound states or mesonlike resonances [8], and (iii) an attractive Coulomb interaction [9]. Recently, the BESIII Collaboration has observed the nonzero cross section near threshold in the process $e^+e^- \to \Lambda\bar{\Lambda}$ [10]. Naturally, it is also interesting to explore the production behavior of Λ_c^+, the lightest baryon containing the charm quark. Previously, the Belle Collaboration measured the cross section of $e^+e^- \to \Lambda_c^+\bar{\Lambda}_c^-$ using the initial-state radiation (ISR) technique [11], but the results suffer from significant uncertainties in c.m. energy and cross section. Therefore, near $\Lambda_c^+\bar{\Lambda}_c^-$ threshold, precise

measurements of the production cross section and EMFF ratios are highly desirable.

In this work, the cross section of the reaction $e^+e^- \to \Lambda_c^+\bar{\Lambda}_c^-$ is measured at four c.m. energies: $\sqrt{s} = 4574.5$, 4580.0, 4590.0, and 4599.5 MeV. At each c.m. energy, ten Cabibbo-favored hadronic decay modes, $\Lambda_c^+ \to pK^-\pi^+$, pK_S^0, $\Lambda\pi^+$, $pK^-\pi^+\pi^0$, $pK_S^0\pi^0$, $\Lambda\pi^+\pi^0$, $pK_S^0\pi^+\pi^-$, $\Lambda\pi^+\pi^+\pi^-$, $\Sigma^0\pi^+$, and $\Sigma^+\pi^+\pi^-$, as well as the ten corresponding charge-conjugate modes are independently used to reconstruct Λ_c^+ or $\bar{\Lambda}_c^-$. Each mode will produce one measurement of the cross section, and the total cross section is obtained from a weighted average over the 20 individual measurements. In addition, the higher statistics data samples at $\sqrt{s} = 4574.5$ and 4599.5 MeV enable the study of the polar angle distribution of Λ_c in the c.m. system. From these distributions, the ratios between the electric and the magnetic form factors, i.e., $|G_E/G_M|$, are extracted for the first time.

The data samples are collected with the BESIII detector [12] at BEPCII. The detector has a geometrical acceptance of 93% of the 4π solid angle. It contains a small-celled, helium-based main drift chamber (MDC), a time-of-flight system (TOF) based on plastic scintillators, an electromagnetic calorimeter (EMC) made of CsI(Tl) crystals, a muon system (MUC) made of resistive plate chambers, and a superconducting solenoid magnet.

Monte Carlo (MC) simulations based on GEANT4 [13] are performed to determine detection efficiencies, optimize selection criteria, extract signal shapes, and study backgrounds. The e^+e^- collisions are simulated by the KKMC generator [14], which takes the beam energy spread and the ISR correction into account. The distribution of the Λ_c polar angle is considered in the generator by parametrizing it with the function $f(\theta) \propto 1 + \alpha_{\Lambda_c}\cos^2\theta$. After an iterative procedure, the values of α_{Λ_c} at $\sqrt{s}$=4574.5 and 4599.5 MeV are obtained from real data (see Table IV) and at the remaining c.m. energies by a linear interpolation.

Using the branching fractions (BR) measured in Ref. [15], all tagged Λ_c decays are simulated by weighting phase-space events according to the decay behavior observed in real data. The subsequent decays listed by the Particle Data Group (PDG) [16] are modeled with EVTGEN [17]. The inclusive MC samples include $\Lambda_c^+\bar{\Lambda}_c^-$ pair production, $\ell^+\ell^-$ ($\ell = e, \mu, \tau$) events, open charm processes [18], ISR-produced low-mass ψ states, and the continuum process $e^+e^- \to q\bar{q}(q = u, d, s)$.

Charged tracks as well as the intermediate states π^0, K_S^0, Λ, Σ^0, and Σ^+ are selected and reconstructed with the same method described in Ref. [15].

In the final states of decay modes $pK_S^0\pi^0$ and $pK_S^0\pi^+\pi^-$, potential background from $\Lambda \to p\pi^-$ is eliminated by rejecting events with $M_{p\pi^-}$ lying in the mass window $(1100, 1125)$ MeV/c^2, where $M_{p\pi^-}$ is the invariant mass of $p\pi^-$ combinations in the final state. For the decay mode $\Sigma^+\pi^+\pi^-$, the corresponding exclusion window is $(1110, 1120)$ MeV/c^2 due to the smaller observed width of the $M_{p\pi^-}$ peak in data. Similarly, background from the intermediate state Σ^+ is removed from the $pK_S^0\pi^0$ sample by rejecting events with $M_{p\pi^0}$ in the mass window $(1170, 1200)$ MeV/c^2. In modes $\Lambda\pi^+\pi^+\pi^-$ and $\Sigma^+\pi^+\pi^-$, events with $M_{\pi^+\pi^-}$ within $(490, 510)$ MeV/c^2 are rejected to suppress the K_S^0 background.

According to energy and momentum conservation, two discriminating variables, the *energy difference* ΔE and the *beam-constrained mass* $M_{\rm BC}$, are utilized to identify the Λ_c signals. The energy difference is defined as $\Delta E \equiv E - E_{\rm beam}$, where E is the energy of the Λ_c candidate and $E_{\rm beam}$ is the mean energy of the two colliding beams. In each tagged mode, the Λ_c candidates are formed by all possible combinations of the final-state particles, and only the one with minimum $|\Delta E|$ is stored. In the following analysis, events are rejected if they fail the ΔE requirements specified in Ref. [15]. The beam-constrained mass is defined as $M_{\rm BC}c^2 \equiv \sqrt{E_{\rm beam}^2 - p^2c^2}$, where p is the momentum of the Λ_c candidate. Both ΔE and $M_{\rm BC}$ are calculated in the initial e^+e^- c.m. system. In Fig. 1, the $M_{\rm BC}$ distributions for $\Lambda_c^+ \to pK^-\pi^+$ at the four c.m. energies are shown. Clear peaks at the nominal Λ_c^+ mass are observed. Studies of the inclusive MC samples show that the cross feeds among the ten tagged modes are less than 1.5%, and the background shape can be described by the ARGUS function [19].

Performing an unbinned maximum likelihood fit to each $M_{\rm BC}$ distribution gives the corresponding event yields, as partly illustrated in Fig. 1. The signal shape of the fit is

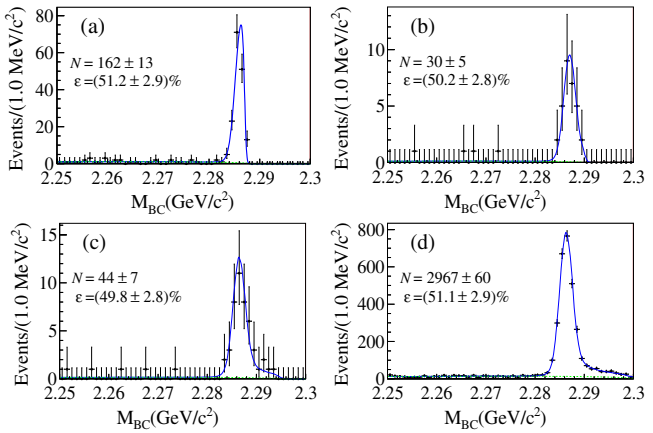

FIG. 1. Fit results of the $M_{\rm BC}$ distribution of $\Lambda_c^+ \to pK^-\pi^+$ in data at (a) $\sqrt{s} = 4574.5$ MeV, (b) 4580.0 MeV, (c) 4590.0 MeV, and (d) 4599.5 MeV. Dots are Poisson averages of the data in the bins, and error bars represent one time of corresponding standard deviations; the blue solid curves are the sum of fit functions, while the barely visible green dashed lines are the background shapes. N is the yield with statistical uncertainty of the Λ_c^+ signal, and ε represents the corresponding detection efficiency and uncertainty.

obtained from convolving the $M_{\rm BC}$ shape of MC simulations with a Gaussian function to compensate a possible resolution difference between data and MC simulations. The background is described by an ARGUS function with the high-end truncation fixed. At $\sqrt{s} = 4599.5$ MeV, the parameters of the ARGUS and the Gaussian functions used in the convolution are obtained from the fit. At the remaining c.m. energies, all parameters obtained at the highest energy, except for the mean of the Gaussian, are used to fix parameters in the new fits. Yields are extracted from the signal region 2276 MeV $< M_{\rm BC}c^2 < E_{\rm beam}$ in each fit. The detection efficiency of each decay mode is evaluated by MC simulations of the $e^+e^- \to \Lambda_c^+\bar{\Lambda}_c^-$ process. Figure 1 gives the efficiencies of mode $pK^-\pi^+$ at the four c.m. energies.

The cross section of the ith mode is determined using

$$\sigma_i = \frac{N_i}{\varepsilon_i \mathcal{L}_{\rm int} f_{\rm VP} {\rm BR}_i f_{\rm ISR}}, \quad (2)$$

where N_i and ε_i represent the yield and corresponding detection efficiency. The integrated luminosity $\mathcal{L}_{\rm int}$ is taken from Refs. [20,21]. The vacuum polarization (VP) correction factor $f_{\rm VP}$ is calculated to be 1.055 at all four c.m. energies [22]. ${\rm BR}_i$ represents the product of branching fractions of the ith Λ_c decay mode and its subsequent decay (s). $f_{\rm ISR}$ is the ISR correction factor derived in Ref. [23] and implemented in KKMC. Since the calculation of $f_{\rm ISR}$ requires the cross-section line shape as input, an iterative procedure has been performed.

The systematic uncertainties of the cross section can be classified into *reconstruction-related* and *general* contributions. The reconstruction-related contributions are mode specific and mainly originate from tracking, PID, reconstruction of intermediate states, and total BRs. The uncertainties of ΔE and $M_{\rm BC}$ requirements are negligible after correcting for the difference in resolution between simulated and real data samples. The uncertainties from the tracking and PID of charged particles are investigated using control samples from $e^+e^- \to \pi^+\pi^-\pi^+\pi^-$, $K^+K^-\pi^+\pi^-$, and $p\bar{p}\pi^+\pi^-$ collected at $\sqrt{s} > 4.0$ GeV [24]. The uncertainties are obtained after weighting according to the momenta of the corresponding final states. Reconstruction uncertainties of K_S^0, Λ, and π^0 have been found to be 1.2%, 2.5%, and 1.0% [15]. Statistical uncertainties of detection efficiencies are considered as systematic uncertainties. The dependence of the reconstruction efficiency on the MC model for the ten decay modes also gives a small contribution to the systematic uncertainty [15]. Uncertainties originating from the total BRs of the tagged modes are quoted from Refs. [15,16]. A summary of the reconstruction-related systematic uncertainties is given in Table I. The total uncertainty at each energy has been calculated assuming that the values given at $\sqrt{s} = 4599.5$ MeV are valid at all c.m. energies.

TABLE I. Summary of the reconstruction-related, mode-specific, relative systematic uncertainties of the cross section at $\sqrt{s} = 4599.5$ MeV, quoted in percentages.

Source	Tracking	PID	K_S^0	Λ	π^0	MC statistic	Signal model	Total BR
$pK^-\pi^+$	3.2	4.6	···	···	···	0.2	···	6.0
pK_S^0	1.3	0.5	1.2	···	···	0.6	0.2	5.6
$\Lambda\pi^+$	1.0	1.0	···	2.5	···	0.8	0.5	6.2
$pK^-\pi^+\pi^0$	3.0	7.6	···	···	1.0	0.6	2.0	8.3
$pK_S^0\pi^0$	1.0	1.8	1.2	···	1.0	1.1	1.0	7.5
$\Lambda\pi^+\pi^0$	1.0	1.0	···	2.5	1.0	0.6	0.6	6.0
$pK_S^0\pi^+\pi^-$	2.8	5.3	1.2	···	···	1.0	0.5	9.3
$\Lambda\pi^+\pi^+\pi^-$	3.0	3.0	···	2.5	···	0.9	0.8	7.9
$\Sigma^0\pi^+$	1.0	1.0	···	2.5	···	1.1	1.7	6.7
$\Sigma^+\pi^+\pi^-$	3.0	4.0	···	···	1.0	0.8	0.8	7.4

The general contributions to the systematic uncertainty originate from uncertainties in $f_{\rm ISR}$, $f_{\rm VP}$, and $\mathcal{L}_{\rm int}$ in Eq. (2) and are the same for all decay modes. The $f_{\rm ISR}$ is obtained using the KKMC generator, which requires a cross-section line shape as input. The line shape is in turn obtained by an iterative fitting procedure of the cross-section data using Eq. (1). In the fit, the $|G_E/G_M|$ value at an arbitrary c.m. energy is assigned by linear interpolation between the two known values listed in Table IV. For simplicity, $|G_M|$ is assumed to be independent of the c.m. energy. To precisely describe the data, the α in the Sommerfeld resummation factor is replaced by $\alpha_s (= 0.25)$. In the line shape, the cross section at the c.m. energy region $(2m_{\Lambda_c}c^2, 4574.5)$ MeV is obtained from extrapolating the fit; below threshold it vanishes, as shown by the blue solid curve in Fig. 2. Four sources of systematic uncertainty from the $f_{\rm ISR}$ are

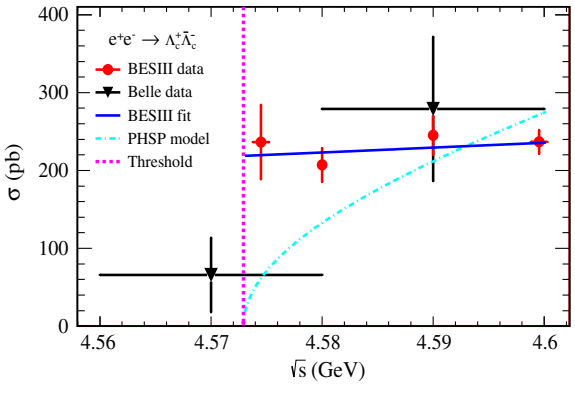

FIG. 2. Cross section of $e^+e^- \to \Lambda_c^+\bar{\Lambda}_c^-$ obtained by BESIII (this work) and Belle. The blue solid curve represents the input line shape for KKMC when determining the $f_{\rm ISR}$. The dash-dotted cyan curve denotes the prediction of the phase-space (PHSP) model, which is parametrized by Eq. (1), but with $C = 1$ and flat $|G_M|$ with respect to $\sqrt{s}$.

TABLE II. Summary of the general relative systematic uncertainties of the cross section originating from the factors $f_{\rm ISR}$, $f_{\rm VP}$, and $\mathcal{L}_{\rm int}$, quoted in percentages.

	$f_{\rm ISR}$						
$\sqrt{s}$ (MeV)	Calculation model	Line shape	C.m. energy	Energy spread	Total	$f_{\rm VP}$	$\mathcal{L}_{\rm int}$
4574.5	3.4	1.2	18.0	3.0	18.6	0.5	1.0
4580.0	0.7	0.6	⋯	0.2	0.9	0.5	0.7
4590.0	0.2	1.7	⋯	⋯	1.7	0.5	0.7
4599.5	0.1	2.6	⋯	⋯	2.6	0.5	1.0

considered: First, the uncertainty of the *calculation model* is studied using a different algorithm mentioned in Ref. [25]. Second, the uncertainty associated with the input *line shape* is estimated using different fit functions. Third, the $f_{\rm ISR}$ depends on the c.m. energy of the $e^+e^- \to \Lambda_c^+\bar{\Lambda}_c^-$ process. The uncertainty of the *c.m. energy* therefore contributes near the threshold. At the lowest energy point, the c.m. energy is measured to be $\sqrt{s} = 4574.50 \pm 0.72$ MeV [26]. Finally, the beam *energy spread*, which has been estimated as 1.55 ± 0.18 MeV, is important near threshold and contributes to the $f_{\rm ISR}$ uncertainty. For the other, higher, energies, the effects from the c.m. energy uncertainty and the beam energy spread are less than 0.1% and can be neglected due to the flat line shape of the cross section. The uncertainty of $f_{\rm VP}$ is calculated to be 0.5% at all four c.m. energies [22]. The uncertainty from the integrated luminosity has been found to be 0.7% at $\sqrt{s} =$ 4580.0 and 4590.0 MeV, and 1.0% at $\sqrt{s} = 4574.5$ and 4599.5 MeV [20,21]. A summary of the general contributions to the systematic uncertainties is given in Table II.

The cross sections obtained in different decay modes are combined using the method mentioned in Ref. [27], in which the cross section is given by

$$\sigma = \sum_i w_i \sigma_i \quad \text{with} \quad w_i = (1/\Delta\sigma_i^2) \Big/ \left(\sum_i 1/\Delta\sigma_i^2\right). \quad (3)$$

Here, w_i and $\Delta\sigma_i$ denote the weight and the total uncertainty, respectively, of the measured cross section σ_i of mode i. The sum is performed over all 20 decay modes

TABLE III. The average cross section of $e^+e^- \to \Lambda_c^+\bar{\Lambda}_c^-$ measured at each c.m. energy, where the uncertainties are statistical and systematic, respectively. The observed cross section can be obtained by multiplying the $f_{\rm ISR}$ and the σ.

$\sqrt{s}$ (MeV)	$\mathcal{L}_{\rm int}$ (pb^{-1})	$f_{\rm ISR}$	σ (pb)
4574.5	47.67	0.45	$236 \pm 11 \pm 46$
4580.0	8.54	0.66	$207 \pm 17 \pm 13$
4590.0	8.16	0.71	$245 \pm 19 \pm 16$
4599.5	566.93	0.74	$237 \pm 3 \pm 15$

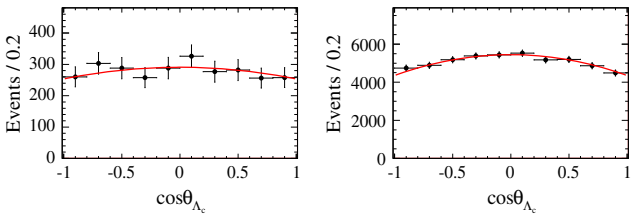

FIG. 3. Angular distribution after efficiency correction and results of the fit to data at $\sqrt{s} = 4574.5$ MeV (left) and 4599.5 MeV (right).

of Λ_c^+ and $\bar{\Lambda}_c^-$ [28]. The combined uncertainty is calculated by

$$\Delta\sigma^2 = \sum_{i,j} w_i (\mathbf{M}_\sigma)_{ij} w_j, \quad (4)$$

where $\mathbf{M}_\sigma$ represents the covariance matrix of these cross-section measurements, in which the correlations between any two measurements σ_i and σ_j are considered. The resulting cross sections at the four c.m. energies are listed in Table III and shown in Fig. 2 together with the Belle data [11] for comparison.

The data sets collected at $\sqrt{s} = 4574.5$ and 4599.5 MeV are large enough to perform a detailed study in the c.m. frame of the Λ_c polar angle θ_{Λ_c}, which is defined as the angle between the Λ_c momentum and the beam direction. The data fulfilling all selection criteria are divided into ten bins in $\cos\theta_{\Lambda_c^+}$. In each $\cos\theta_{\Lambda_c^+}$ bin, the total yield is obtained by summing the yields of all the ten tagged modes. The one-dimensional bin-by-bin efficiency corrections are applied on these total yields. The same procedure is performed by tagging $\bar{\Lambda}_c^-$ decay channels. The total yields of Λ_c^+ and $\bar{\Lambda}_c^-$ are combined bin-by-bin, and the shape function $f(\theta) \propto (1 + \alpha_{\Lambda_c} \cos^2\theta)$ is fitted to the combined data, as shown in Fig. 3. Table IV lists the resulting α_{Λ_c} parameters obtained from the fits, as well as the $|G_E/G_M|$ ratios extracted using the equation

$$|G_E/G_M|^2(1-\beta^2) = (1-\alpha_{\Lambda_c})/(1+\alpha_{\Lambda_c}). \quad (5)$$

The systematic uncertainties of the α_{Λ_c} considered here are the contributions from the fit range and the bin size. A change of the fit range in $\cos\theta$ from $(-1.0, 1.0)$ to $(-0.8, 0.8)$ and in the number of bins from 10 to 20 is performed, and the differences in the obtained α_{Λ_c} are regarded as the systematic uncertainty. Systematics

TABLE IV. Shape parameters of the angular distribution and $|G_E/G_M|$ ratios at $\sqrt{s} = 4574.5$ and 4599.5 MeV. The uncertainties are statistical and systematic, respectively.

$\sqrt{s}$ (MeV)	α_{Λ_c}	$\lvert G_E/G_M \rvert$
4574.5	$-0.13 \pm 0.12 \pm 0.08$	$1.14 \pm 0.14 \pm 0.07$
4599.5	$-0.20 \pm 0.04 \pm 0.02$	$1.23 \pm 0.05 \pm 0.03$

originating from the model dependencies in the efficiency correction are found to be negligible compared to the statistical uncertainties.

In summary, using data collected at $\sqrt{s} = 4574.5$, 4580.0, 4590.0, and 4599.5 MeV with the BESIII detector, the cross sections of $e^+e^- \to \Lambda_c^+\bar{\Lambda}_c^-$ have been measured with high precision, by reconstructing Λ_c^+ and $\bar{\Lambda}_c^-$ independently with ten Cabibbo-favored hadronic decay channels. The most precise cross-section measurement is achieved so far at $\sqrt{s} = 4574.5$ MeV, which is only 1.6 MeV above the threshold. The measured value is $(236 \pm 11 \pm 46)$ pb, which highlights the enhanced cross section near threshold and indicates the complexity of production behavior of the Λ_c. At $\sqrt{s} = 4574.5$ and 4599.5 MeV, the data samples are large enough to study polar angle distributions of Λ_c and measure the Λ_c form-factor ratio $|G_E/G_M|$ for the first time. These results provide important insights into the production mechanism and structure of the Λ_c baryons.

The BESIII Collaboration thanks the staff of BEPCII, the IHEP computing center and the supercomputing center of USTC for their strong support. This work is supported in part by the National Key Basic Research Program of China under Contract No. 2015CB856700; the National Natural Science Foundation of China (NSFC) under Contracts No. 11235011, No. 11335008, No. 11375205, No. 11425524, No. 11625523, No. 11635010, No. 11322544, No. 11375170, No. 11275189, No. 11475164, No. 11475169, No. 11605196, and No. 11605198; the Chinese Academy of Sciences (CAS) Large-Scale Scientific Facility Program; the CAS Center for Excellence in Particle Physics (CCEPP); Joint Large-Scale Scientific Facility Funds of the NSFC and CAS under Contracts No. U1332201, No. U1532257, No. U1532258, and No. U1532102; CAS under Contracts No. KJCX2-YW-N29, No. KJCX2-YW-N45, and No. QYZDJ-SSW-SLH003; the 100 Talents Program of CAS; the National 1000 Talents Program of China; INPAC and Shanghai Key Laboratory for Particle Physics and Cosmology; German Research Foundation DFG under Collaborative Research Center Contracts No. CRC 1044 and No. FOR 2359; Istituto Nazionale di Fisica Nucleare, Italy; Koninklijke Nederlandse Akademie van Wetenschappen (KNAW) under Contract No. 530-4CDP03; the Ministry of Development of Turkey under Contract No. DPT2006K-120470; the National Natural Science Foundation of China (NSFC) under Contracts No. 11505034 and No. 11575077; the National Science and Technology fund; the Swedish Research Council; the U.S. Department of Energy under Contracts No. DE-FG02-05ER41374, No. DE-SC-0010118, No. DE-SC-0010504, and No. DE-SC-0012069; the University of Groningen (RuG) and the Helmholtzzentrum fuer Schwerionenforschung GmbH (GSI), Darmstadt; and the WCU Program of the National Research Foundation of Korea under Contract No. R32-2008-000-10155-0.

[a]Also at Bogazici University, 34342 Istanbul, Turkey.
[b]Also at the Moscow Institute of Physics and Technology, Moscow 141700, Russia.
[c]Also at the Functional Electronics Laboratory, Tomsk State University, Tomsk, 634050, Russia.
[d]Also at the Novosibirsk State University, Novosibirsk, 630090, Russia.
[e]Also at the NRC "Kurchatov Institute," PNPI, 188300, Gatchina, Russia.
[f]Also at Istanbul Arel University, 34295 Istanbul, Turkey.
[g]Also at Goethe University Frankfurt, 60323 Frankfurt am Main, Germany.
[h]Also at Key Laboratory for Particle Physics, Astrophysics and Cosmology, Ministry of Education; Shanghai Key Laboratory for Particle Physics and Cosmology; Institute of Nuclear and Particle Physics, Shanghai 200240, People's Republic of China.
[i]Government College Women University, Sialkot 51310, Punjab, Pakistan.

[1] R. Pohl *et al.*, Nature (London) **466**, 213 (2010).
[2] N. Cabibbo and R. Gatto, Phys. Rev. **124**, 1577 (1961).
[3] A. Sommerfeld, Ann. Phys. (Berlin) **403**, 257 (1931); S. J. Brodsky and R. F. Lebed, Phys. Rev. Lett. **102**, 213401 (2009).
[4] A. D. Sakharov, Sov. Phys. Usp. **34**, 375 (1991).
[5] J. P. Lees *et al.* (*BABAR* Collaboration), Phys. Rev. D **87**, 092005 (2013); **88**, 072009 (2013).
[6] M. Ablikim *et al.* (BESIII Collaboration), Phys. Rev. D **91**, 112004 (2015).
[7] O. D. Dalkarov, P. A. Khakhulin, and A. Y. Voronin, Nucl. Phys. **A833**, 104 (2010).
[8] B. El-Bennich, M. Lacombe, B. Loiseau, and S. Wycech, Phys. Rev. C **79**, 054001 (2009); J. Haidenbauer, H. W. Hammer, U.-G. Meißner, and A. Sibirtsev, Phys. Lett. B **643**, 29 (2006).
[9] R. Baldini, S. Pacetti, A. Zallo, and A. Zichichi, Eur. Phys. J. A **39**, 315 (2009); R. Baldini, S. Pacetti, and A. Zallo, Eur. Phys. J. A **48**, 33 (2012).
[10] M. Ablikim *et al.* (BESIII Collaboration), Phys. Rev. D **97**, 032013 (2018).
[11] G. Pakhlova *et al.* (Belle Collaboration), Phys. Rev. Lett. **101**, 172001 (2008).
[12] M. Ablikim *et al.* (BESIII Collaboration), Nucl. Instrum. Methods Phys. Res., Sect. A **614**, 345 (2010).
[13] S. Agostinelli *et al.* (GEANT4 Collaboration), Nucl. Instrum. Methods Phys. Res., Sect. A **506**, 250 (2003).
[14] S. Jadach, B. F. L. Ward, and Z. Wąs, Comput. Phys. Commun. **130**, 260 (2000).
[15] M. Ablikim *et al.* (BESIII Collaboration), Phys. Rev. Lett. **116**, 052001 (2016).
[16] C. Patrignani *et al.* (Particle Data Group), Chin. Phys. C **40**, 100001 (2016).
[17] D. J. Lange, Nucl. Instrum. Methods Phys. Res., Sect. A **462**, 152 (2001); R. G. Ping, Chin. Phys. C **32**, 599 (2008).

[18] N. Brambilla *et al.*, Eur. Phys. J. C **71**, 1534 (2011).
[19] H. Albrecht *et al.* (ARGUS Collaboration), Phys. Rev. Lett. **241**, 278 (1990).
[20] M. Ablikim *et al.* (BESIII Collaboration), Chin. Phys. C **39**, 093001 (2015).
[21] M. Ablikim *et al.* (BESIII Collaboration), Chin. Phys. C **41**, 063001 (2017).
[22] S. Actis *et al.*, Eur. Phys. J. C **66**, 585 (2010); F. Jegerlehner, Z. Phys. C **32**, 195 (1986).
[23] S. Jadach, B. F. L. Ward, and Z. Wąs, Phys. Rev. D **63**, 113009 (2001).
[24] M. Ablikim *et al.* (BESIII Collaboration), Phys. Rev. Lett. **117**, 232002 (2016).
[25] R. G. Ping *et al.*, Chin. Phys. C **40**, 113002 (2016).
[26] M. Ablikim *et al.* (BESIII Collaboration), Chin. Phys. C **40**, 063001 (2016).
[27] M. Schmelling, Phys. Scr. **51**, 676 (1995).
[28] At $\sqrt{s} = 4599.5$ MeV, the deviations between any two of the 20 individual Born cross section can be covered by corresponding total uncertainty. However, this is not the case for a few decay channels at the other three energies due to the low statistics of the data sample.